









Spiral copropagation of two relativistic intense laser beams in a plasma channel

Huanyu Song ^{1,2} Zhengming Sheng ^{1,2,3,*} Hanzhi Zhao ^{1,2} Xiangyan An ^{1,2} Suming Weng ^{1,2} Min Chen ^{1,2}
Tongpu Yu ⁴ and Jie Zhang ^{1,2,3,5}

¹Key Laboratory for Laser Plasmas (MOE), School of Physics and Astronomy, Shanghai Jiao Tong University, Shanghai 200240, China

²Collaborative Innovation Center of IFSA (CICIFSA), Shanghai Jiao Tong University, Shanghai 200240, China

³Tsung-Dao Lee Institute, Shanghai Jiao Tong University, Shanghai 201210, China

⁴Department of Physics, National University of Defense Technology, Changsha 410073, China

⁵Beijing National Laboratory for Condensed Matter Physics, Institute of Physics, Chinese Academy of Sciences, Beijing 100190, China



(Received 15 May 2023; revised 24 May 2023; accepted 11 October 2023; published 2 November 2023)

The copropagation of two relativistic intense laser beams with orthogonal polarization in a parabolic plasma channel is studied analytically and numerically. A set of coupled equations for the evolution of the laser spot sizes and transverse centroids are derived by use of the variational approach. It is shown that the centroids of the two beams can spiral and oscillate around each other along the channel axis, where the characteristic frequency is determined both by the laser and plasma parameters. The results are verified by direct numerical solution of the relativistic nonlinear Schrödinger equations for the laser envelopes as well as three-dimensional particle-in-cell simulations. In the case with two ultrashort laser pulses when laser wakefields are excited, it is shown that the two wake bubbles driven by the laser pulses can spiral and oscillate around each other in a way similar to the two pulses. This can be well controlled by adjusting the incidence angle and separation distance between the two laser pulses. Preliminary studies show that externally injected electron beams can follow the trajectories of the oscillating bubbles. Our studies suggest a new way to control the coupling of two intense lasers in plasma for various applications, such as electron acceleration and radiation generation.

DOI: [10.1103/PhysRevE.108.055202](https://doi.org/10.1103/PhysRevE.108.055202)

I. INTRODUCTION

The propagation of intense laser beams in plasma is broadly interesting because of their relevance to laser-driven accelerators [1,2], laser plasma-based undulators [3,4], advanced laser fusion schemes [5], etc. To guide the laser propagation over a long distance, a preformed plasma channel is usually used [6,7]. It is well known that if the laser pulse enters the channel off-axis or under some angle, the laser beam centroid will oscillate with an oscillation period about the Rayleigh length range during its propagation [8]. In this case, the wake bubble driven by an ultrashort laser pulse will follow the trajectory of the laser. This leads to the trapped and accelerated electrons undergoing transverse betatron oscillations, which produce tunable radiation in the x-ray range [9,10]. In addition, centroid oscillations can also occur when multiple laser beams interact with each other. When two relativistic intense laser beams propagate in an underdense plasma, the interaction features are determined by their polarization. For the same polarization, Dong *et al.* found that two laser beams can merge into one beam or split into three beams under different cases [11]. Huang *et al.* showed that distinct interaction features, attraction, repulsion, and energy shift are induced by controlling the relative phase between the two laser pulses [12]. Particularly, for orthogonal polarization, by using the

variational approach, Ren *et al.* illustrated the spiral motion of two laser beams [13,14]. Wu *et al.* studied the oscillation features by including both the relativistic electron-mass correction and the ponderomotive force effect [15]. These studies suggest that two orthogonally polarized laser beams can spiral or oscillate around each other without a plasma channel. In this case, however, the mutual attraction force between the two beams is very weak and easily destroyed by modulational instability and kinetic effects [16]. Therefore, generally it is difficult to clearly observe the spiral motion and oscillation motion of the two beams in homogeneous plasma.

Even though the laser centroid oscillations are found in previous studies when a single laser beam enters the plasma channel off-axis [17,18] or when two laser beams copropagate in homogeneous plasma, the propagation characteristics of two laser beams in a parabolic plasma channel are not explored yet. In addition, it is not yet clear that the evolution features of two wake bubbles, which are generated by two laser pulses, oscillate transversely in a plasma channel. In this paper, we focus on the copropagation of the two orthogonally polarized laser beams in a parabolic plasma channel. We address this problem analytically first based upon the envelope equations described by the coupled relativistic nonlinear Schrödinger equations (NLSE) and by resorting to the variational approach developed in Refs. [14,19]. This approach gives the evolution equations of two laser beam centroids and spot sizes. It is found that the two beams can spiral and oscillate around each other, where the frequency is determined by laser-plasma parameters. The analytical findings are further

*Author to whom correspondence should be addressed: zmsheng@sjtu.edu.cn

confirmed by solving the coupled NLSE numerically as well as by three-dimensional (3D) particle-in-cell (PIC) simulations. Furthermore, we investigate the evolution features of two wake bubbles driven by two relativistic ultrashort laser pulses in a plasma channel. It is demonstrated that the evolution of the two bubbles can be controlled by adjusting the laser conditions. Under the appropriate laser-plasma parameters, the two bubbles can follow the trajectories of two laser pulses, where the spiral motion or transverse oscillation motion of the bubbles along the channel axis is found. In addition, we show that externally injected electron beams can follow the trajectories of the oscillating bubbles.

The paper is organized as follows. In Sec. II, the spiral motion and transverse oscillation motion of two laser beams are analyzed using the variational approach. In Sec. III, 3D PIC simulations and NLSE simulations are conducted to verify the conclusions obtained in Sec. II. In Sec. IV, we extend our studies to the short-pulse regime, where the evolution features of two wake bubbles and externally injected electron beams in a plasma channel are analyzed. A brief summary is given finally in Sec. V.

II. THEORY MODEL ON THE LASER CENTROID MOTION

The density profile of a parabolic plasma channel [20] is written as $n_e = n_0(1 + \alpha r^2/r_{ch}^2)$. Here n_0 refers to the plasma density along the channel axis, α describes the steepness of the plasma channel, and r_{ch} denotes the transverse size of the plasma channel. Our physical model is based on the long laser pulse approximation starting from the Maxwell's equations. In the slowly varying envelope approximation and paraxial approximation, the coupled relativistic NLSE equations [21,22] for two laser beams with orthogonal polarization

in a parabolic plasma channel can be written as

$$\left(2ik_0 \frac{\partial}{\partial z} + \nabla_{\perp}^2 - k_p^2 \alpha \frac{r^2}{r_{ch}^2}\right) a_{1,2} = -k_p^2 \left(1 - \frac{n}{\gamma}\right) a_{1,2}, \quad (1)$$

which is given in the laser group velocity frame (z, τ, r) with $\tau = t - z/v_g$ and z the laser propagation direction. Here $\nabla_{\perp}^2 = \partial^2/\partial x^2 + \partial^2/\partial y^2$ is the Laplace operator, $k_0 = \omega_0/c$ is the wave vector of the laser beam, ω_0 is the laser frequency, c is the vacuum light speed, $k_p = \omega_p/c$, ω_p is the plasma frequency, and $r^2 = y^2 + x^2$. The lasers are described by the complex amplitude of the electric field $a_{1,2} = eE_{1,2}/m_e\omega_0c$, m_e is the electron rest mass, and $\gamma = \sqrt{1 + (|a_1|^2 + |a_2|^2)/2}$ is the relativistic factor. In order to avoid the nonphysical value of the plasma density [22], the normalized density is given by $n = n_e/n_0 = \max(0, 1 + k_p^{-2}\nabla_{\perp}^2\gamma)$, where we have assumed the ions act as homogeneous positive background. It is noted that our physical model has considered both the relativistic effect and the ponderomotive expulsion of the electrons. At the weakly relativistic approximation, $n/\gamma \approx 1 - \frac{1}{4}(1 - \nabla_{\perp}^2)(|a_1|^2 + |a_2|^2)$. Substituting n/γ into Eq. (1), one obtains the following equation:

$$\begin{aligned} &\left(2ik_0 \frac{\partial}{\partial z} + \nabla_{\perp}^2 - k_p^2 \alpha \frac{r^2}{r_{ch}^2}\right) a_{1,2} \\ &= -\frac{k_p^2}{4} a_{1,2} (1 - \nabla_{\perp}^2)(|a_1|^2 + |a_2|^2). \end{aligned} \quad (2)$$

It is impossible to obtain exact solutions to Eq. (2) because of the nonlinear terms. The approximate solution of Eq. (2) can be obtained by using the variational approach. By finding a Lagrangian density \mathcal{L} and minimizing the action $\int_{-\infty}^{\infty} \mathcal{L} dz dx dy$, one can reproduce Eq. (2). Such a Lagrangian density is

$$\begin{aligned} \mathcal{L} = &\sum_{j=1,2} \left\{ ik_0 \left(a_j \frac{\partial a_j^*}{\partial z} - a_j^* \frac{\partial a_j}{\partial z} \right) + \nabla_{\perp} a_j^* \cdot \nabla_{\perp} a_j - k_p^2 \left[\frac{|a_j|^4}{8} + \frac{(\nabla_{\perp} |a_j|^2)^2}{8} - \alpha \frac{(x^2 + y^2)|a_j|^2}{r_{ch}^2} \right] \right\} \\ &- \frac{k_p^2}{4} (|a_1|^2 \cdot |a_2|^2 + \nabla_{\perp} |a_1|^2 \cdot \nabla_{\perp} |a_2|^2). \end{aligned} \quad (3)$$

Next we choose the following trial function for each laser beam

$$a_j = a_{0j} \exp(-i\phi_j) \exp\{-i[k_{xj}(x - X_{cj}) + k_{yj}(y - Y_{cj})]\} \exp\{[(x - X_{cj})^2 + (y - Y_{cj})^2](ik_0/2R_j - 1/W_j^2)\}, \quad (4)$$

where the amplitude a_{0j} , phase ϕ_j , beam center (X_{cj}, Y_{cj}) , perpendicular momentum (k_{xj}, k_{yj}) , radius of curvature R_j , and the beam radius W_j are all real and are functions of z only. Substituting the trial function into Eq. (3) and integrating the Lagrangian density over the xy plane, we obtain a reduced Lagrangian (additional details are presented in the Appendix)

$$\begin{aligned} L \equiv &\frac{2}{\pi} \int_{-\infty}^{\infty} dx \int_{-\infty}^{\infty} dy \mathcal{L} \\ = &\sum_{j=1,2} \left\{ -\frac{k_0 a_{0j}^2 W_j^2}{4} \left[8 \frac{d\phi_j}{dz} + \frac{2k_0 W_j^2}{R_j^2} \frac{dR_j}{dz} - 8 \left(k_{xj} \frac{dX_{cj}}{dz} + k_{yj} \frac{dY_{cj}}{dz} \right) \right] \right. \\ &+ \frac{a_{0j}^2}{4} \left[\frac{2k_0^2 W_j^4}{R_j^2} + 8 + 4W_j^2 (k_{xj}^2 + k_{yj}^2) \right] - \frac{k_p^2 a_{0j}^4}{4} - \frac{k_p^2 a_{0j}^4 W_j^2}{16} + \frac{\alpha k_p^2 a_{0j}^2 W_j^2}{2r_{ch}^2} (W_j^2 + 2X_{cj}^2 + 2Y_{cj}^2) \left. \right\} \\ &- k_p^2 a_{01}^2 a_{02}^2 \frac{W_1^2 W_2^2}{W_1^2 + W_2^2} \exp\left(\frac{-2d^2}{W_1^2 + W_2^2}\right) \left[\frac{1}{4} + \frac{2}{W_1^2 + W_2^2} - \frac{4d^2}{(W_1^2 + W_2^2)^2} \right]. \end{aligned} \quad (5)$$

Here d is the distance between the centers of the two beams, $d^2 = (X_{c1} - X_{c2})^2 + (Y_{c1} - Y_{c2})^2$. When the reduced action is minimized, one can find the evolution equations of the beam parameters by the Euler-Lagrange equations for the reduced Lagrangian density $\partial L/\partial \beta - (d/dz)\partial L/\partial \dot{\beta} = 0$, where β is any parameter for the laser beam given in Eq. (4). Varying ϕ_j leads to power conservation $d(a_{0j}^2 W_j^2)/dz = 0$. This prompts us to obtain a conserved quantity $P_j = a_{0j}^2 W_j^2$. Varying R_j gives $W_j/R_j = dW_j/dz$. Varying W_j gives equations for the evolution of spot sizes

$$\begin{aligned} \frac{d^2 W_j}{dz^2} + \frac{4}{k_0^2 W_j^3} \left(\frac{P_j k_p^2}{32} - 1 \right) + \frac{k_p^2 P_j}{k_0^2 W_j^5} + \frac{k_p^2 \alpha W_j}{k_0^2 r_{ch}^2} \\ = \frac{k_p^2 P_1 P_2 W_j}{2k_0^2 (W_1^2 + W_2^2)^2 P_j} \exp\left(\frac{-2d^2}{W_1^2 + W_2^2}\right) \left(-1 + \frac{2d^2}{W_1^2 + W_2^2}\right) + \frac{8k_p^2 P_1 P_2 W_j}{k_0^2 (W_1^2 + W_2^2)^3 P_j} \exp\left(\frac{-2d^2}{W_1^2 + W_2^2}\right) \left(-1 + \frac{d^2}{W_1^2 + W_2^2}\right) \\ - \frac{8k_p^2 P_1 P_2 W_j d^2}{k_0^2 (W_1^2 + W_2^2)^4 P_j} \exp\left(\frac{-2d^2}{W_1^2 + W_2^2}\right) \left(-3 + \frac{2d^2}{W_1^2 + W_2^2}\right). \end{aligned} \quad (6)$$

The motion of the beam centroids can be obtained from varying (k_{xj}, k_{yj}) and (X_{cj}, Y_{cj}) . Varying (k_{xj}, k_{yj}) lead to $dX_{cj}/dz = -k_{xj}/k_0$ and $dY_{cj}/dz = -k_{yj}/k_0$. With the small angle approximation, we can obtain $k_{xj}/k_0 = \theta_{xj}$ and $k_{yj}/k_0 = \theta_{yj}$. Here, θ_{xj} and θ_{yj} are the beam's initial incidence angle with respect to the x axis and y axis, respectively. While varying Y_{cj} , one obtains the following equations:

$$P_1 \frac{d^2 Y_{c1}}{dz^2} = -\frac{k_p^2 \alpha P_1}{k_0^2 r_{ch}^2} Y_{c1} - \frac{2k_p^2 P_1 P_2 (Y_{c1} - Y_{c2})}{k_0^2 (W_1^2 + W_2^2)^2} \exp\left(-\frac{2d^2}{W_1^2 + W_2^2}\right) \left[\frac{1}{4} + \frac{4}{W_1^2 + W_2^2} - \frac{4(Y_{c1} - Y_{c2})^2}{(W_1^2 + W_2^2)^2} \right], \quad (7a)$$

$$P_2 \frac{d^2 Y_{c2}}{dz^2} = -\frac{k_p^2 \alpha P_2}{k_0^2 r_{ch}^2} Y_{c2} + \frac{2k_p^2 P_1 P_2 (Y_{c1} - Y_{c2})}{k_0^2 (W_1^2 + W_2^2)^2} \exp\left(-\frac{2d^2}{W_1^2 + W_2^2}\right) \left[\frac{1}{4} + \frac{4}{W_1^2 + W_2^2} - \frac{4(Y_{c1} - Y_{c2})^2}{(W_1^2 + W_2^2)^2} \right]. \quad (7b)$$

Similar equations hold in the x direction. In a simplified case, assuming $P_1 = P_2 = P = a_0^2 W^2$, $W_1 = W_2 = W$, and $a_{01} = a_{02} = a_0$. After some straightforward algebra, one obtains the following equations of motion

$$\frac{d^2 \Delta X_c}{dz^2} = -\frac{k_p^2}{k_0^2} \left[\frac{P}{W^4} \left(\frac{1}{4} + \frac{2}{W^2} - \frac{d^2}{W^4} \right) \exp\left(-\frac{d^2}{W^2}\right) + \frac{\alpha}{r_{ch}^2} \right] \Delta X_c, \quad (8a)$$

$$\frac{d^2 \Delta Y_c}{dz^2} = -\frac{k_p^2}{k_0^2} \left[\frac{P}{W^4} \left(\frac{1}{4} + \frac{2}{W^2} - \frac{d^2}{W^4} \right) \exp\left(-\frac{d^2}{W^2}\right) + \frac{\alpha}{r_{ch}^2} \right] \Delta Y_c, \quad (8b)$$

where $\Delta X_c = X_{c1} - X_{c2}$, $\Delta Y_c = Y_{c1} - Y_{c2}$, and $d^2 = (\Delta X_c)^2 + (\Delta Y_c)^2$. We consider two simple types of solutions to Eqs. (8a) and (8b). One possibility is that the distance between the two beams d is a constant, that is, the two beams spiral around each other. In this case, Eqs. (8a) and (8b) have known solutions

$$\Delta X_c = \Delta X_{c0} \cos \Omega_{sl} z + (\Delta \theta_x / \Omega_{sl}) \sin \Omega_{sl} z, \quad (9a)$$

$$\Delta Y_c = \Delta Y_{c0} \cos \Omega_{sl} z + (\Delta \theta_y / \Omega_{sl}) \sin \Omega_{sl} z, \quad (9b)$$

where ΔX_{c0} and ΔY_{c0} is the initial centroid displacement with respect to the x axis and y axis, respectively, $\Delta \theta_x = \theta_{x1} - \theta_{x2}$, $\Delta \theta_y = \theta_{y1} - \theta_{y2}$, and Ω_{sl} is the spiral frequency given by

$$\Omega_{sl} = \sqrt{\frac{k_p^2 a_0^2}{k_0^2 W^2} \left(\frac{1}{4} + \frac{2}{W^2} - \frac{d^2}{W^4} \right) \exp\left(-\frac{d^2}{W^2}\right) + \frac{k_p^2 \alpha}{k_0^2 r_{ch}^2}}. \quad (10)$$

Consider the most straightforward case of the spiral motion $\Delta X_c = (\Delta \theta_x / \Omega_{sl}) \sin \Omega_{sl} z$, $\Delta Y_c = \Delta Y_{c0} \cos \Omega_{sl} z$, and let $\Delta Y_{c0} = \Delta \theta_x / \Omega_{sl}$. The physical picture is schematically shown in Fig. 1. The two beams spiral around each other, and the distance d is a constant. In addition, one notes that the spiral frequency Ω_{sl} is contributed by two terms, i.e., the two-beam

coupling term $N_t = \frac{k_p^2 a_0^2}{k_0^2 W^2} \left(\frac{1}{4} + \frac{2}{W^2} - \frac{d^2}{W^4} \right) \exp\left(-\frac{d^2}{W^2}\right)$ and the plasma channel term $C_t = k_p^2 \alpha / k_0^2 r_{ch}^2$. In order to gain a full view of the relative magnitudes of these two terms, we define a ratio parameter $\xi = C_t / N_t$. It can be seen from Fig. 2(a) that the ratio parameter ξ increases dramatically with the spot size W and the plasma channel α / r_{ch}^2 . That is, the plasma channel C_t is dominant when W and α / r_{ch}^2 are large enough. Otherwise, the two-beam coupling term N_t is dominant. The curves in Fig. 2(b) show the ratio parameter ξ as a function of the separation distance d at different spot sizes. This indicates that with the increase of separation distance between the two laser beams, ξ can also increase, which means the two-beam coupling term becomes weak rapidly. But the larger the spot sizes, the slower the increase of the ratio parameter.

Another type of solution occurs when two copropagating beams are parallel to each other. In this case, they will oscillate transversely in a two-dimensional plane and the oscillation is also coupled to the spot size evolution of Eq. (6). Since the distance d is variable, one cannot obtain the oscillation frequency Ω_{os} as above. If the spot-size change is neglected, one can obtain the Ω_{os} by numerically solving the Eq. (7) with the fourth-order Runge-Kutta method. Furthermore, our analytical model neglects certain kinetic effects in the plasma,

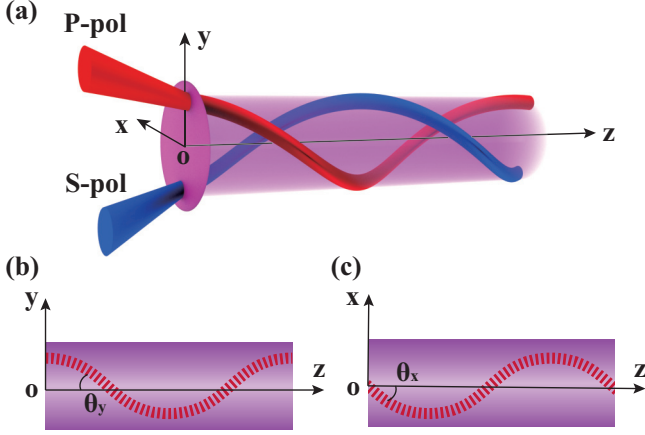


FIG. 1. Schematic of the spiral motion of two relativistic intense laser beams with orthogonal polarization, where the laser electric field is along the x axis for the p polarization and it is along the y axis for the s polarization. The two lasers are launched obliquely into a parabolic plasma channel, θ_x and θ_y are the angles between the laser propagation direction and the space coordinate axes x , y .

such as electron acceleration and corresponding quasistatic magnetic field generation [23], etc. Usually, these effects are significant in plasma with moderate densities and laser intensities, but relatively weak in tenuous plasma [24]. Thus, the results described above should apply preferably in tenuous plasma, for example, $n_e \leq 0.01n_c$.

III. 3D-PIC SIMULATIONS AND NLSE SIMULATIONS

In this section, 3D PIC simulations and NLSE simulations are employed to test the validity of our theoretical analysis and display the propagation characteristics of the two laser beams directly. The 3D PIC simulations are conducted using the EPOCH code [25]. The simulation box is of size $400 \times 40 \times 40 \mu\text{m}$, which consists of $4000 \times 200 \times 200$ cells and each cell contains 4 macro particles. In the NLSE simulations, Eq. (1) is numerically solved with the algorithm of the alternating-direction implicit method [26,27], where a rectangular simulation box is used in the x - y plane with the

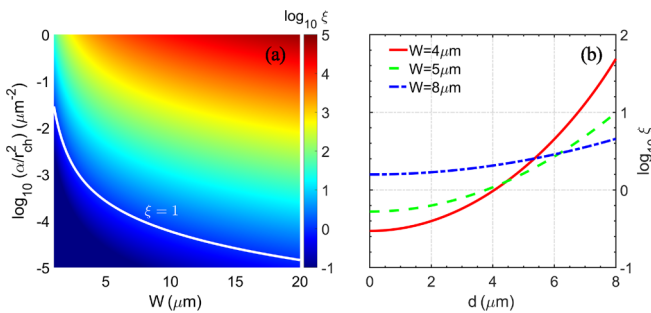


FIG. 2. (a) The ratio parameter ξ as a function of the spot size W and plasma channel parameter α/r_{ch}^2 , where $a_0 = 0.25$ and $d = W$. Note that we use logarithmic coordinates for α/r_{ch}^2 and ξ , the white line represents $\xi = 1$. (b) The ratio parameter ξ as a function of the separation distance d for different spot sizes W , where $a_0 = 0.6$ and $\alpha/r_{ch}^2 = 1/400 \mu\text{m}^{-2}$.

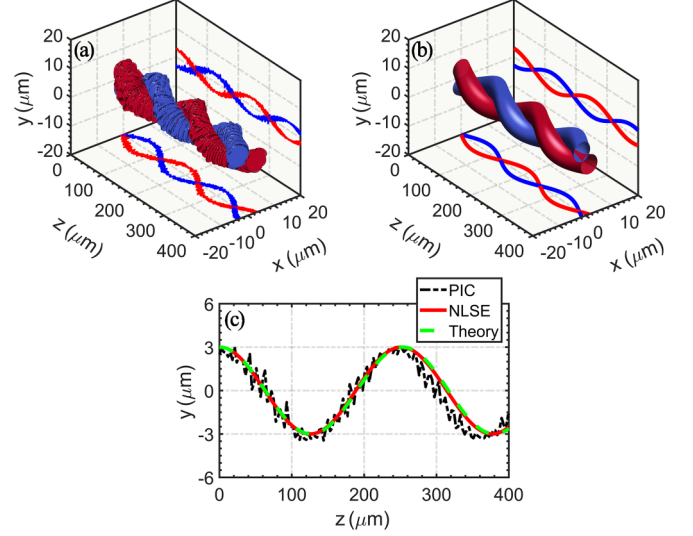


FIG. 3. Isosurface of vector potential at $a = a_0/4$ of the p -polarized laser (red beam) and the s -polarized laser (blue beam) obtained by PIC simulation (a) and NLSE simulation (b) for the spiral motion. The lines on the box walls are projections of the centroids. (c) Theoretical (green dashed line) result, NLSE simulation (red solid line) and PIC simulation (black dash dot line) of the centroid trajectory of the p -polarized laser in the y - z plane. The initial laser parameters are $a_0 = 0.25$, $W_0 = 3 \mu\text{m}$, and $d = 6 \mu\text{m}$.

size of $40 \times 40 \mu\text{m}$. Apparently, from Eq. (6), it is not easy to choose appropriate laser-plasma parameters to just satisfy the stationary spot sizes requirement [18]. For simplicity, the spot-sizes change is neglected; the spot sizes are assumed to be constant as laser beams propagate. In the following 3D simulations, we do find that the laser spot sizes are almost unchanged. For the spiral motion, two linearly polarized Gaussian laser beams, one with p polarization (laser electric field is parallel to the plane of incidence) and another with s polarization (laser electric field is perpendicular to the plane of incidence), are obliquely launched into the simulation box along the z axis. The initial transverse profiles of the two laser beams are $a_{1,2} = a_0 \exp(-[(y - Y_{c1,2})^2 + x^2]/W_0^2)$, where the peak normalized vector potential $a_0 = 0.25$, initial laser spot size or the beam waist in vacuum $W_0 = 3 \mu\text{m}$, $Y_{c1} = -Y_{c2} = 3 \mu\text{m}$, and the separation distance $d = 6 \mu\text{m}$ correspondingly. The laser wavelength is set as $\lambda_0 = 1 \mu\text{m}$, the plasma density has a channel profile with $n_0 = 0.01n_c$, and $\alpha/r_{ch}^2 = 1/16 \mu\text{m}^{-2}$. From Eq. (10), we can obtain the spiral frequency (wavenumber) $\Omega_{sl} = 0.025 \lambda_0^{-1}$ and the spiral period $\Lambda_{sl} = 2\pi/\Omega_{sl} = 251.3 \mu\text{m}$ correspondingly. Thus, we set the incident angle $\theta_{x1} = -\theta_{x2} = 0.075$. In this case, $\xi = 1.32e^{-4}$, implying that the two-beam coupling term is very weak and the plasma channel term is dominant. In the whole simulation process, the centroids $\langle x \rangle_i$ and $\langle y \rangle_i$ of the two beams are tracked, where $\langle x \rangle_i = I_{\text{tot}}^{-1} \int_{-\infty}^{\infty} x |a_i(x, y)|^2 dx dy$, $\langle y \rangle_i = I_{\text{tot}}^{-1} \int_{-\infty}^{\infty} y |a_i(x, y)|^2 dx dy$, and $I_{\text{tot}} = \int_{-\infty}^{\infty} |a_i(x, y)|^2 dx dy$, which represents the total laser energy.

The spiral motion is clearly shown in Fig. 3, where the red beam is p -polarized and the blue beam is s -polarized. The isosurface of vector potential is $a = a_0/4$. Figures 3(a)

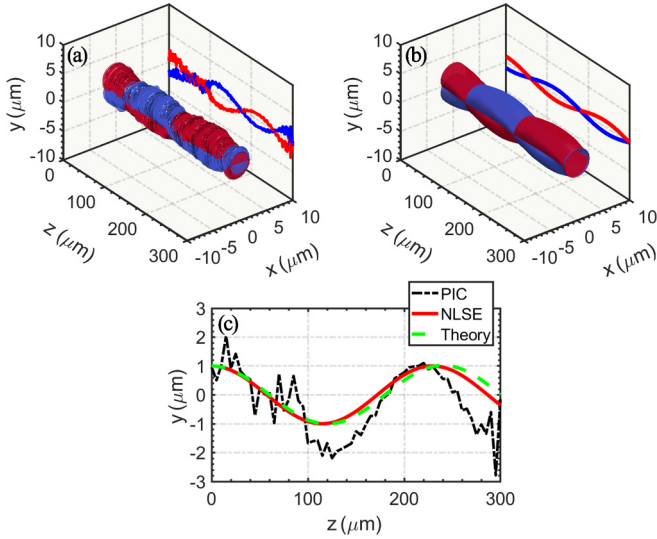


FIG. 4. Isosurface of vector potential at $a = a_0/6$ of the p -polarized laser (red beam) and the s -polarized laser (blue beam) obtained by PIC simulation (a) and NLSE simulation (b) for the oscillation motion. (c) Theoretical (green dashed line) result, NLSE simulation (red solid line), and PIC simulation (black dash dot line) of the centroid trajectory of the p -polarized laser in the y - z plane. The initial laser parameters are $a_0 = 0.60$, $W = 3 \mu\text{m}$, and $d = 2 \mu\text{m}$.

and 3(b) correspond to PIC simulation and NLSE simulation, respectively. The solid lines are the projections of centroid trajectories on x - z and y - z planes. In Fig. 3(c), the green dashed line shows typical trajectory of the laser centroid obtained from Eqs. (9) and (10). The black line and red line represent the centroid trajectories of p -polarized laser in the y - z plane from PIC simulation and NLSE simulation, respectively. As one can see, the spiral period is about $245 \mu\text{m}$ from the PIC simulation and $251 \mu\text{m}$ from the NLSE simulation, which are very close to the analytical solution $\Lambda_{sl} = 251.3 \mu\text{m}$ given by Eq. (10). In the PIC simulation, because of the laser energy depletion and laser deformation as the laser beams propagate further, the period is slightly smaller than the theoretical prediction.

When two beams propagate parallel to each other, they will oscillate around each other. Simulation parameters are as follows: $a_0 = 0.6$, $Y_{c1} = -Y_{c2} = 1 \mu\text{m}$, $W_0 = 3 \mu\text{m}$, $n_0 = 0.01n_c$, and $\alpha/r_{ch}^2 = 1/16 \mu\text{m}^{-2}$. In this case, the interaction of two beams plays an important role in oscillation frequency. It is shown from Figs. 4(a) and 4(b) that the two beams attract, intersect, separate, and stably copropagate in the plasma channel. By numerically solving the Eqs. (7a) and (7b) with the fourth-order Runge-Kutta method, one finds that the two beams have a cosinoidal oscillation motion, where its oscillation frequency (wavenumber) $\Omega_{os} = 0.0274 \lambda_0^{-1}$ and oscillation period $\Lambda_{os} = 2\pi/\Omega_{os} = 229.4 \mu\text{m}$, as shown with the green dashed line in Fig. 4(c). In the PIC simulation, the oscillation period is about $220 \mu\text{m}$, which is slightly lower than the theoretical results. We should point out that 3D simulations are time-consuming and thus longitudinal grid resolution ($\Delta x = 0.1 \mu\text{m}$) is set a little low in our cases. Therefore, the centroid trajectories from the PIC simulation are not smooth due to some numerical errors. It is important

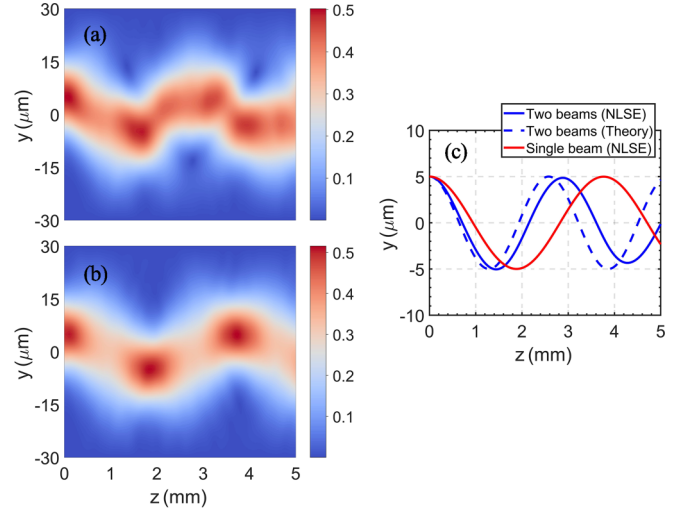


FIG. 5. Evolution of the p -polarized laser in the y - z plane for two laser beams case (a) and for single beam case (b). The color bar is a_0 . (c) Centroid trajectory of the p -polarized laser for the two beams case (blue solid line) and for the single beam case (red solid line), and theoretical result (blue dashed line).

to mention that although we ignore the change of the laser spot sizes, the theoretical results agree well with the simulation results, which indicates that the laser spot sizes remain almost constant under our simulation parameters.

In examples shown above, the plasma channel effect is dominant. We also investigate a case where the two-beam coupling effect dominates. The simulation parameters are as follows: $a_0 = 0.5$, $Y_{c1} = -Y_{c2} = 5 \mu\text{m}$, $W_0 = 10 \mu\text{m}$, $n_0 = 0.01n_c$, and $\alpha/r_{ch}^2 = 1/3600 \mu\text{m}^{-2}$. In this case, the channel effect becomes rather weak and the two-beam coupling effect plays an important role in oscillation motion. By solving Eqs. (7a) and (7b) numerically, one finds that the theoretical oscillation period is about 2.58 mm , as shown with the dashed line in Fig. 5(c). It is almost impossible for us to carry out a 3D PIC simulation because of the huge amount of computation resources required for this case. Therefore, we use NLSE simulations to demonstrate the propagation characteristics of the two laser beams. Figure 5(a) shows the evolution of p -polarized laser beam in the y - z plane when there are two laser beams; the oscillation period is 2.89 mm [see Fig. 5(c)], the spot size evolves slightly in the whole process. As a comparison, the single laser case is also considered [Fig. 5(b)], in which the oscillation period (about 3.77 mm) is much increased compared to the two lasers case. This implies that the oscillation period can be much reduced in the presence of the two-beam coupling effect.

The above results show our theoretical model agrees well with the simulations both for the spiral motion and oscillation motion, especially for the case with strong channel effect. However, our simulations show that the theoretical results would slightly deviate from the simulation results when the plasma channel term is relatively weak as compared to the two-beam coupling term. In this case, there is a considerable change in the beam spot sizes as found in the simulations, which is difficult to be taken into account in our theoretical model [see Eq. (6)]. This is similar to the findings in Ref. [15],

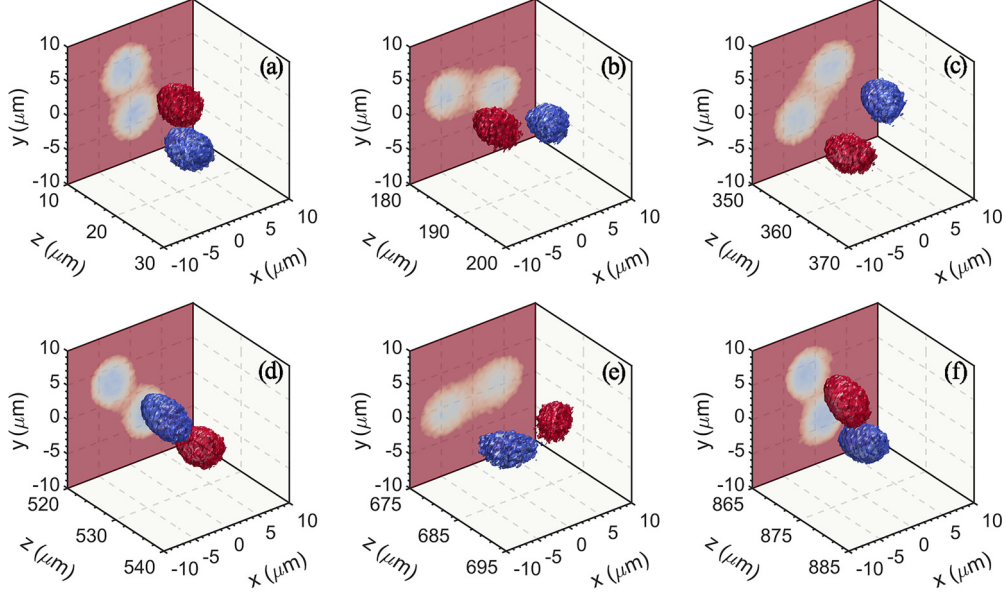


FIG. 6. Isosurface of the plasma electron density profiles (at $n_e = 0.002n_c$) associated with the spiraling plasma bubbles generated by a p -polarized laser (red color) and a s -polarized laser (blue color) at $t = 40T_0$ (a), $t = 260T_0$ (b), $t = 480T_0$ (c), $t = 700T_0$ (d), $t = 900T_0$ (e), $t = 1140T_0$ (f), respectively. The projections on x - y plane show the spiral motion of the two bubbles.

where the interaction of two copropagating laser beams has been studied in the homogeneous plasma.

IV. EVOLUTION OF TWO WAKE BUBBLES INSIDE A PLASMA CHANNEL

Our theory and simulation shown in the previous sections are valid for long laser pulses. Now we extend our studies to the regime of ultrashort intense pulses. When an ultrashort, relativistic intensity laser pulse propagates in plasma, the background electrons are expelled outward due to the ponderomotive force of the laser pulse, generating bubblelike wakefields [1,28]. If the laser pulse oscillates transversely in a plasma channel, the bubble and trapped electrons, if existing, will follow the trajectories of the laser pulse, which can be used as a radiation source. Combined Laguerre-Gaussian laser has been recently suggested to generate twisted wake structures, resulting in spiraling electron trajectories around the twisted wakefield [29–31]. So far, the evolution of these twisted wake bubbles generated by regular linearly polarized laser beams has not been investigated. In this section, by using 3D EPOCH code, we examine the evolution features of two wake bubbles, which are generated by two orthogonally polarized laser pulses inside a parabolic plasma channel with different laser conditions. The simulations use a moving window. The simulation box is of size $50 \times 40 \times 40 \mu\text{m}$, which consists of $1000 \times 400 \times 400$ cells and each cell contains 4 macroparticles. Two orthogonally polarized lasers are incident into the simulation box at an initial separation distance d . The lasers have wavelength $\lambda_0 = 0.8 \mu\text{m}$ and normalized laser vector potential $a_{1,2} = a_0 \exp[-(t - L_0)^2/L_0^2] \exp[-[(y - Y_{c1,2})^2 + x^2]/W_0^2]$, with $a_0 = 1.4$, $L_0 = 8.0T_0$, $W_0 = 5.5 \mu\text{m}$, $Y_{c1} = -Y_{c2} = 4 \mu\text{m}$, and the separation distance $d = 8 \mu\text{m}$, correspondingly. The laser period $T_0 = 2\pi/\omega_0 \approx 2.67 \text{ fs}$. The plasma density has a parabolic profile with $n_0 = 0.003n_c$, $\alpha/r_{ch}^2 = 1/64 \mu\text{m}^{-2}$,

where $n_c \approx 1.7 \times 10^{21} \text{ cm}^{-3}$ is the critical plasma density for the laser pulses.

According to Eq. (9), if we set $\theta_{x1} = -\theta_{x2} = 0.0292$, the two laser pulses can spiral around each other with the spiral period $\Lambda_{sl} = 865.9 \mu\text{m}$. In this case, the evolutions of the two wake bubbles and the projections of the bubble cross sections at different times are shown in Fig. 6, where the isosurface of density $n_e = 0.002n_c$ appears as two separate ellipsoids. The red color represents the bubble generated by the p -polarized laser and blue color represents the bubble generated by the s -polarized laser. As can be seen from Fig. 6(a), shortly after the injection of the two laser pulses into the plasma, two wake bubbles are formed at about $t = 40T_0$. Because of the spiral motion of the two lasers, the two bubbles will also spiral around each other anticlockwise, as depicted in Fig. 6(b). And then, the spiral copropagation of the two bubbles remains stable in the plasma channel, as shown in Figs. 6(c)–6(f). From Figs. 6(a) and 6(f), one sees that the spiral period from the PIC simulation is about $855 \mu\text{m}$, close to that predicted by our analytical model.

When we set the incident angle $\theta_{x1} = -\theta_{x2} = 0$, the two laser pulses can oscillate around each other with the oscillation period $\Lambda_{os} = 809.5 \mu\text{m}$ according to Eq. (7). Typical bubble evolutions and bubble cross sections at different laser propagation distances are plotted in Fig. 7. It is shown from Fig. 7(a) that the two wake bubbles are stably generated at about $t = 40T_0$. As the two lasers approach each other, the two bubbles start to merge, as depicted in Fig. 7(b). At $t = 280T_0$, the two lasers completely merge into a single laser, accompanied by the merging of two bubbles into a single bubble [Fig. 7(c)]. In the next stage, the two merged lasers start to be separated and, correspondingly, the merged bubble also gradually splits into two, as shown in Fig. 7(d). One sees that the colors of the two bubbles are switched, because the p -polarized laser is at the top and the s -polarized laser is at the bottom at this time. And then, similar evolution occurs

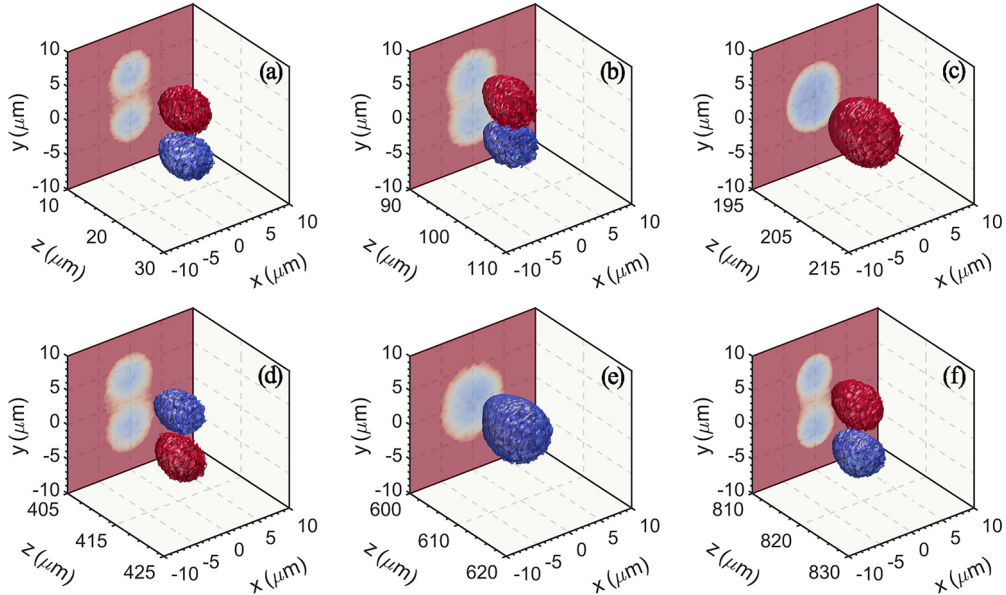


FIG. 7. Isosurface of the plasma electron density profiles (at $n_e = 0.002n_c$) associated with the oscillating plasma bubbles generated by a p -polarized laser (red color) and a s -polarized laser (blue color) at $t = 40T_0$ (a), $t = 140T_0$ (b), $t = 280T_0$ (c), $t = 550T_0$ (d), $t = 800T_0$ (e), $t = 1070T_0$ (f), respectively. The projections on x - y plane show the oscillation motion of the two bubbles.

again with the bubbles merging and separating [Figs. 7(e) and 7(f)]. After that, the process described above is repeated periodically until the laser pulses become strongly distorted and depleted. Furthermore, it is noted from Figs. 7(a) and 7(f) that the oscillation period of the two bubbles is about $800 \mu\text{m}$, which is consistent with our analytical model.

The above results show that with appropriate laser and plasma parameters, spiraling or oscillating motion of two plasma bubbles can appear and their period can be controlled. In principle, the trapped electrons, if existing, will undergo transverse betatron oscillations in wakefields, which lead to the betatron radiation in the x-ray range. As the radiation power and frequency are proportional to the number of trapped electrons, betatron oscillation amplitudes, and periods [3,32], the spiraling or oscillation copropagation of the two laser pulses/plasma bubbles provide additional control of the betatron radiation power and frequency spectra.

As an example, we illustrate the copropagation of two trapped electron bunches in two separated plasma bubbles, which carry out betatron oscillations in a plasma channel. To reduce simulation time and concentrate on the study of the trajectories of trapped electrons in such oscillating plasma bubbles, we simply consider externally injected electron beams by using two-dimensional PIC simulations. The beams have transverse size of $0.5 \mu\text{m}$ and longitudinal length of $1.2 \mu\text{m}$. The simulation box is of size $40 \times 40 \mu\text{m}$, which consists of 1000×400 cells and each cell contains 36 macroparticles. We take the peak amplitude $a_0 = 1.8$, the pulse duration $L_0 = 6.7 fs$, other parameters such as plasma density, laser spot size, and their separation distance are the same as shown above in this section. Figure 8(a) illustrates the evolution of the laser field (dark blue), plasma density (red), and externally injected electrons (brown) at different positions. At the beginning of the interaction, the externally injected electrons are trapped at the back of the bubbles. Following the merging of the bubbles, the two bunches

approach each other and gradually merge [Fig. 8(b)]. And then, the merged bubble gradually splits into two; the merged electron bunch also separate and follow the trajectories of the two bubbles [Figs. 8(c) and 8(d)]. After that, the process described above is repeated periodically until the electrons enter the dephasing region.

V. DISCUSSION AND SUMMARY

It should be pointed out that, in the case of highly relativistic laser intensity with strong bubble effects as shown in Sec. IV, our analytical model is less accurate. However, we still observe the spiral motion or oscillation motion of the two wake bubbles with their period approximately

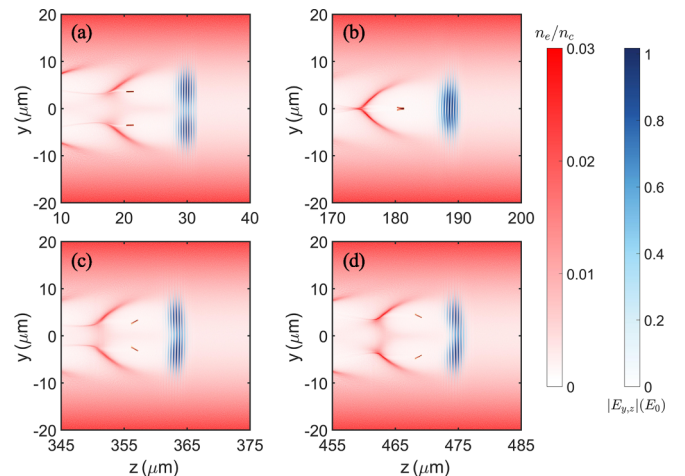


FIG. 8. Distribution of absolute value of the transverse laser electric fields (dark blue, in units of E_0), electron density n_e (red background, in units of n_c) and externally injected electrons (brown) at $t = 40T_0$ (a), $t = 240T_0$ (b), $t = 460T_0$ (c), $t = 600T_0$ (d).

consistent with our analytical model. We have also considered the small separation distance between the two laser pulses, e.g., $d = 4.0 \mu\text{m}$. The interesting finding is that, instead of following the trajectories of the two laser pulses, the two wake bubbles attract each other, always merging to a single bubble along the channel axis. The above phenomena can also be found in the case with a higher laser intensity of $a_0 = 2.0$. In this case, more complicated bubble structures are formed [33]. In addition, we find that it is better to keep $Y_c/W < 1$ in our simulations. Otherwise, the laser pulses may experience severe deformation and no stable bubble structures can be formed [34]. Finally, we believe that electron injection and the radiation properties in such two wake bubbles are an interesting issue as well. To avoid excessive expansion of our current paper, we leave the details for future studies.

In summary, the copropagation of two orthogonally polarized laser beams in a parabolic plasma channel has been investigated analytically and numerically. It is found that the variational approach correctly predicts the period of spiral motion and oscillation motion for the typical propagation distances in our investigation, both in good agreement with 3D PIC simulations and NLSE simulations. In this way, it is possible to manipulate the propagation dynamics of two laser beams by controlling laser-plasma parameters. For ultrashort laser pulses, it is shown that by controlling the incidence angle and initial separation distance between the two laser pulses, distinct evolution features of the two wake bubbles, such as spiraling, merging, and splitting periodically, are illustrated with their period well described by our analytical model. Moreover, externally injected electrons inside the bubbles can follow the motion of laser centroids. This may provide the possibility to control the electron acceleration process in plasma, which could be interesting for optimizing the properties of associated x-ray radiation.

ACKNOWLEDGMENTS

This work was supported by National Natural Science Foundation of China (Grants No. 12135009 and No.

11991074). The simulations were performed on the π 2.0 supercomputer at Shanghai Jiao Tong University.

APPENDIX

In this Appendix, we present some auxiliary calculations leading to the Lagrangian of Eq. (5). Compared with Ref. [14], the plasma channel effect and ponderomotive force effect are considered in this study. The Lagrangian density of plasma channel effect can be written as $\mathcal{L}_{\text{chan}} = \sum_{j=1,2} k_p^2 \alpha (x^2 + y^2) |a_j|^2 / r_{ch}^2$, here $|a_j|^2 = a_{0j}^2 \exp\{-2[(x - X_{cj})^2 + (y - Y_{cj})^2] / W_j^2\}$, $j = 1, 2$. Using the Gaussian integral $\int_{-\infty}^{\infty} e^{-\alpha(x-x_1)^2} x^2 dx = \sqrt{\pi} (1 + 2\alpha x_1^2) / 2\alpha^{3/2}$ and after some integral operation, we obtain the integrated Lagrangian

$$\mathcal{L}_{\text{chan}} = \sum_{j=1,2} \alpha k_p^2 a_{0j}^2 W_j^2 (W_j^2 + 2X_{cj}^2 + 2Y_{cj}^2) / 2r_{ch}^2.$$

The Lagrangian density of ponderomotive force effect can be written as

$$\mathcal{L}_{\text{pond}} = \sum_{j=1,2} -\frac{k_p^2 \nabla_{\perp} |a_j|^2 \cdot \nabla_{\perp} |a_j|^2}{8} - \frac{k_p^2 \nabla_{\perp} |a_1|^2 \cdot \nabla_{\perp} |a_2|^2}{4}.$$

The integrated Lagrangian of the first term is $-k_p^2 a_{0j}^4 / 4$. For the second term, using the Gaussian integral $\int_{-\infty}^{\infty} e^{\alpha(x-x_1)^2 + \beta(x-x_2)^2} x^2 dx = \sqrt{\frac{\pi}{-(\alpha+\beta)}} e^{\frac{\alpha\beta}{\alpha+\beta}(x_1-x_2)^2}$ and after some complicated integration, we obtain the integrated Lagrangian

$$\begin{aligned} & -\frac{k_p^2 a_{01}^2 a_{02}^2 W_1^2 W_2^2}{W_1^2 + W_2^2} \exp\left(\frac{-2d^2}{W_1^2 + W_2^2}\right) \\ & \times \left[\frac{2}{W_1^2 + W_2^2} - \frac{4d^2}{(W_1^2 + W_2^2)^2} \right]. \end{aligned}$$

Here $d^2 = (X_{c1} - X_{c2})^2 + (Y_{c1} - Y_{c2})^2$. The derivation of other terms is identical with Ref. [14].

-
- [1] T. Tajima and J. M. Dawson, *Phys. Rev. Lett.* **43**, 267 (1979).
[2] W. P. Leemans, B. Nagler, A. J. Gonsalves, Cs Tóth, K. Nakamura, C. G. R. Geddes, E. Esarey, C. B. Schroeder, and S. M. Hooker, *Nature Phys* **2**, 696 (2006).
[3] A. Rousse *et al.*, *Phys. Rev. Lett.* **93**, 135005 (2004).
[4] M. Fuchs *et al.*, *Nature Phys* **5**, 826 (2009).
[5] M. Tabak, J. Hammer, M. E. Glinsky, W. L. Kruer, S. C. Wilks, J. Woodworth, E. M. Campbell, M. D. Perry, and R. J. Mason, *Phys. Plasmas* **1**, 1626 (1994).
[6] C. S. Liu and V. K. Tripathi, *Phys. Plasmas* **1**, 3100 (1994).
[7] E. Esarey, C. B. Schroeder, B. A. Shadwick, J. S. Wurtele, and W. P. Leemans, *Phys. Rev. Lett.* **84**, 3081 (2000).
[8] S. G. Rykovanov, C. B. Schroeder, E. Esarey, C. G. R. Geddes, and W. P. Leemans, *Phys. Rev. Lett.* **114**, 145003 (2015).
[9] M. Chen, J. Luo, F. Y. Li, F. Liu, Z. M. Sheng, and J. Zhang, *Light Sci. Appl.* **5**, e16015 (2016).
[10] J. Luo, M. Chen, M. Zeng, J. Vieira, L. L. Yu, S. M. Weng, L. O. Silva, D. A. Jaroszynski, Z. M. Sheng, and J. Zhang, *Sci. Rep.* **6**, 29101 (2016).
[11] Q. L. Dong, Z. M. Sheng, and J. Zhang, *Phys. Rev. E* **66**, 027402 (2002).
[12] T. W. Huang, C. T. Zhou, R. X. Bai, L. B. Ju, K. Jiang, T. Y. Long, H. Zhang, S. Z. Wu, and S. C. Ruan, *Phys. Rev. E* **98**, 053207 (2018).
[13] C. Ren, B. J. Duda, R. G. Evans, R. A. Fonseca, R. G. Hemker, and W. B. Mori, *Phys. Plasmas* **9**, 2354 (2002).
[14] C. Ren, R. G. Hemker, R. A. Fonseca, B. J. Duda, and W. B. Mori, *Phys. Rev. Lett.* **85**, 2124 (2000).
[15] H. C. Wu, Z. M. Sheng, and J. Zhang, *Phys. Rev. E* **70**, 026407 (2004).
[16] A. Pukhov and J. Meyer-ter Vehn, *Phys. Rev. Lett.* **76**, 3975 (1996).

- [17] S. G. Rykovanov, J. W. Wang, V. Yu. Kharin, B. Lei, C. B. Schroeder, C. G. R. Geddes, E. Esarey, and W. P. Leemans, *Phys. Rev. Accel. Beams* **19**, 090703 (2016).
- [18] E. Esarey, P. Sprangle, J. Krall, and A. Ting, *IEEE J. Quantum Electron.* **33**, 1879 (1997).
- [19] A. V. Buryak, Y. S. Kivshar, M.-f. Shih, and M. Segev, *Phys. Rev. Lett.* **82**, 81 (1999).
- [20] T. W. Huang, C. T. Zhou, H. Zhang, S. Z. Wu, B. Qiao, X. T. He, and S. C. Ruan, *Phys. Rev. E* **95**, 043207 (2017).
- [21] A. B. Borisov, O. B. Shiryaev, A. McPherson, K. Boyer, and C. K. Rhodes, *Plasma Phys. Control. Fusion* **37**, 569 (1995).
- [22] G. Sun, E. Ott, Y. C. Lee, and P. Guzdar, *Phys. Fluids* **30**, 526 (1987).
- [23] Z. M. Sheng and J. Meyer-ter-Vehn, *Phys. Rev. E* **54**, 1833 (1996).
- [24] J. C. Adam, A. Héron, S. Guérin, G. Laval, P. Mora, and B. Quesnel, *Phys. Rev. Lett.* **78**, 4765 (1997).
- [25] T. D. Arber, K. Bennett, C. S. Brady, A. Lawrence-Douglas, M. G. Ramsay, N. J. Sircombe, P. Gillies, R. G. Evans, H. Schmitz, A. R. Bell, and C. P. Ridgers, *Plasma Phys. Control. Fusion* **57**, 113001 (2015).
- [26] W. H. Press and S. A. Teukolsky, *Comput. Phys.* **6**, 188 (1992).
- [27] Z. M. Sheng, K. Nishihara, T. Honda, Y. Sentoku, K. Mima, and S. V. Bulanov, *Phys. Rev. E* **64**, 066409 (2001).
- [28] S. M. Hooker, *Nature Photon* **7**, 775 (2013).
- [29] J. Vieira, J. T. Mendonça, and F. Quéré, *Phys. Rev. Lett.* **121**, 054801 (2018).
- [30] Y. Shi, J. Vieira, R. M. G. M. Trines, R. Bingham, B. F. Shen, and R. J. Kingham, *Phys. Rev. Lett.* **121**, 145002 (2018).
- [31] J. Vieira and J. T. Mendonça, *Phys. Rev. Lett.* **112**, 215001 (2014).
- [32] M. Chen, E. Esarey, C. G. R. Geddes, C. B. Schroeder, G. R. Plateau, S. S. Bulanov, S. Rykovanov, and W. P. Leemans, *Phys. Rev. ST Accel. Beams* **16**, 030701 (2013).
- [33] J. Luo, M. Chen, G.-B. Zhang, T. Yuan, J.-Y. Yu, Z.-C. Shen, L.-L. Yu, S.-M. Weng, C. B. Schroeder, and E. Esarey, *Phys. Plasmas* **23**, 103112 (2016).
- [34] B. Lei, J. Wang, V. Kharin, M. Zepf, and S. Rykovanov, *Phys. Rev. Lett.* **120**, 134801 (2018).